International Journal of Earth Sciences (2023) 112:981–997
https://doi.org/10.1007/s00531-023-02292-8

ORIGINAL PAPER

Discovery of Neoproterozoic adakitic rocks in the Eastern Tianshan (NW China) of the southern Altaids

Meng Wang[1,2,3] · Qigui Mao[1,3] · Wenjiao Xiao[1,3] · He Yang[1,3] · Hao Wang[1,3] · Rui Li[1,3]

Received: 2 April 2022 / Accepted: 10 January 2023 / Published online: 28 January 2023

Abstract

The Paleo-Asian Ocean, as the processor of the Altaids, was a long-lived ocean, and its subduction gave rise to substantial continental growth in the Central Asian continent. However, the location of the major oceanic basin and its evolution history are debatable, impeding our better comprehension of the early accretionary tectonics of the Paleo-Asian Ocean and its link to the reconstruction of the Rodinia. Here, we report our newly discovered Neoproterozoic adakitic rock (Xingxingxia gneissic granite) in the Eastern Tianshan of the southern Altaids to address the above issues. The Xingxingxia gneissic granite displays high Sr/Y ratios (47–114) and strongly fractionated rare earth element (REE) patterns with low concentrations of Y (3.00–6.36 ppm) and Yb (0.23–0.62 ppm), indicative of the adakite affinity. The adakitic rock is depleted in Nb, Ta, P and Ti, and possesses low Mg# (37–42), comparatively high K_2O/Na_2O ratios (0.75–1.08). Zircon U–Pb dating reveal that the adakitic rock was formed at 869 ± 9 Ma, which has relatively depleted Hf isotopic compositions ($\varepsilon_{Hf}(t) = +1.9$ to $+4.7$). Their geochemical features are consistent with those of an origin from a thickened lower arc crust. Our work suggests that subduction of the Paleo-Asian oceanic slab beneath the Central Tianshan Arc occurred at least in the Neoproterozoic. Therefore, our study provides a solid and key evidence to show that the tectonic position of the major Paleo-Asian Ocean was located in the South Tianshan, where the paleo-ocean evolved into its mature stage following the subduction beneath the Central Tianshan at ca. 870 Ma. This work also shed light on the reconstruction of Rodinia and the interaction of the Paleo-Asian Ocean and the Jiangnan–North Tarim Ocean.

Keywords Paleo-Asian Ocean · Eastern Tianshan · CAOB · Rodinia · Neoproterozoic adakitic rock

Introduction

The Altaids, also known as the Altaid Tectonic Collage (Şengör et al. 1993) or the southern Central Asian Orogenic Belt (CAOB), was formed by the largest and longest-lived accretion and convergence of the Kazakhstan, Mongolia and Tarim–North China collage systems (Xiao et al. 2015a). The Paleo-Asian Ocean (PAO) recorded in the Altaids was a long-lived ocean, which was opened during the breakup of the Rodinia supercontinent in the Mesoproterozoic–Neoproterozoic (ca. 1300–700 Ma) (Coney 1992; Dobretsov et al. 2003; Li et al. 2008a; Wan et al. 2018), and its subduction made the Central Asian continent generating considerable continental growth. Therefore, a systematical study on the earlier evolution history of the PAO will shed light on not only the tectonics and continental growth of the Altaids but also the reconstruction of the Rodinia supercontinent.

While the closure timing of the PAO has been extensively studied and relatively well constrained either in the Permian (Liu et al. 2020) or even in the Triassic (Ao et al. 2021; Xiao et al. 2015b), the start of the PAO is not well constrained. Several different views about the start of the PAO have been proposed (Berzin and Dobretsov 1994; Khain and Bozhko 1988; Mossakovskii et al. 1993; Şengör et al. 1993; Şengör and Natal'in 1996), with possible ages only from the late

✉ Qigui Mao
qg_mao@sina.cn

✉ Wenjiao Xiao
wj-xiao@mail.iggcas.ac.cn

1 College of Geography and Remote Sensing Sciences, Xinjiang University, Urumqi 830046, China

2 National Key Laboratory of Arid Area Ecological Security and Sustainable Development, Xinjiang Institute of Ecology and Geography, Chinese Academy of Sciences, Urumqi 830011, China

3 University of Chinese Academy of Sciences, Beijing 100049, China

Neoproterozoic to Paleozoic, and reconstructed the general historical framework of the PAO at ~1000–650, ~650–510, and ~510–450 Ma (Khain et al. 2003). The evidence found in an ophiolite in the accretionary wedge as well as corresponding arc formation in the northern Altaids indicates the evolution of the PAO had begun at least ~1020 Ma ago (Rytsk et al. 2007). The ophiolites at 917 ± 14 Ma in northern Transbaikalia (Gordienko et al. 2009) and at 800 ± 3 Ma in northern Mongolia (Kuzmichev et al. 2005) demonstrate the existence of the PAO since the early Neoproterozoic.

However, the location of the PAO's major oceanic basin and tectonic history of the CAOB remain controversial, particularly because there is no direct evidence for its early evolution, which hampers a better understanding of the tectonics of the Altaids and the reconstruction of the Rodinia supercontinent. Recently, He et al. (2018) reported in *situ* O and Hf isotopes of zircons from the Mesoproterozoic (ca. 1.4 Ga) metabasic amphibolites and granitic rocks from the Chinese Central Tianshan microcontinent in the southern Central Asian Orogenic Belt (CAOB), which provides indirect evidence for Mesoproterozoic (ca. 1.4 Ga) crustal growth constituting a considerable Paleoproterozoic supracrustal component in the Central Tianshan block.

Adakites are usually considered to be derived from the partial melting of metamorphosed mafic rocks or the fractional crystallization of arc-related mafic magmas (Hastie et al. 2021) and therefore, are considered as direct diagnostic evidence for subduction and continental growth. This work focuses on our newly discovered adakite-like gneissic granite at Xingxingxia in the Eastern Tianshan, NW China, in the southern Altaids. In this study, we present zircon U–Pb age and in situ Hf isotopic composition and whole-rock geochemistry of the Xingxingxia gneissic granite, which exhibits adakitic characteristics and is Neoproterozoic in age (ca. 869 Ma). The new discovery of Neoproterozoic adakitic rocks enables us to address the tectonic position of the major Paleo-Asian Ocean and its mature stage with the formation of the subduction zone at ca. 870 Ma, together with its implications for the reconstruction of the Rodinia supercontinent.

Geological background and sampling

The vast Altaids is situated between the Siberian Craton to the north and the Tarim Block to the south and was formed by the amalgamations and accretions of massive continental margin arcs, microcontinents, island arcs, ophiolites, accretionary wedges (Windley et al. 2010; Xiao et al. 2004, 2010; Zuo et al. 1991). The Tianshan orogenic belt is located in the southern Altaids, and is mainly composed of the North Tianshan suture zone, Yili block, Central Tianshan block and South Tianshan suture zone from the north to the south (Fig. 1a) (Charvet et al. 2011; Kröner et al. 2008; Wang et al. 2014b; Windley et al. 2007; Xiao et al. 2010a).

With a long-term accretionary orogeny, several E–W-striking accretionary belts and faults were developed from north to south and the Eastern Tianshan of the Tianshan orogenic belt is composed of several blocks juxtaposed by ophiolitic mélanges (Mao et al. 2021b). In the Eastern Tianshan, the Central Tianshan block is separated from the Tarim block to the south and the North Tianshan tectonic zone to the north by the Kumishi–Hongliuhe suture and the Aqikkudug–Weiya suture, respectively (Guo and Li 1993; Shu et al. 2004) (Fig. 1b).

In the Beishan, several ophiolitic belts were recognized and regarded as the suture zones between the blocks/arcs (Liu and Wang 1995; Nie 2002; Wang et al. 2014a; Xiao et al. 2010b; Zuo 1990; Zuo et al. 1991), which include the Hongshishan, Xingxingxia, Hongliuhe and Liuyuan belts that occur along large-scale faults named after these ophiolitic belts, respectively (Fig. 2). The Hanshan block was proposed to be the eastern part of the eastern Central Tianshan (Liu and Wang 1995; Xiao et al. 2010b; Zuo et al. 1991).

The Central Tianshan block comprises mainly of Precambrian basement with minor amounts of the early and late Paleozoic volcano-sedimentary formations (Hu et al. 2000; Li and Kusky 2007; Liu et al. 2004; Shu et al. 2004; Xiao et al. 2004; Yang et al. 2008) and a number of granitoid intrusions (Fig. 2). The basement contains the Mesoproterozoic Xingxingxia, the Neoproterozoic Tianhu and the Kawabulake Groups, and was subjected to greenschist to amphibolite facies metamorphism, which shows fault and/or unconformable contact relationships to each other (Gao et al. 1993). The widely distributed granitoid intrusions of Proterozoic to Triassic ages mostly share a strong affinity to I-type granites (Gu 2006; Gu et al. 1999; Hu et al. 2007; Wang et al. 2006; Wu et al. 2006; Zhang et al. 2005; Zhang et al. 2007b).

The Xingxingxia Group consisted of banded and augen gneissic granites, marbles, amphibolites, migmatites, quartzites and schists that have experienced metamorphism from greenschist to amphibolite facies, or even to granulite facies at some localities (Li et al. 2007, 2008b; Liu et al. 2004). Hu et al. (2000) suggested that the gneissic granite and amphibolites in the Xingxingxia Group are metamorphosed granitic–mafic plutons or volcanic rocks. The Tianhu Group, located between the Tianhu and Xingxingxia area, which is composed of metamorphic volcanic rocks, carbonates and clastic rocks, with the main components of amphibolite schists, plagioclase gneisses, chloritic quartz schists and migmatites. It shows fault unconformable contact with the Kawabulag Groups (Deng et al. 2017; Liu et al. 2004). The Kawabulake Group generally shows as a shallow sea silica-rich calcium–magnesium carbonate sedimentary sequence

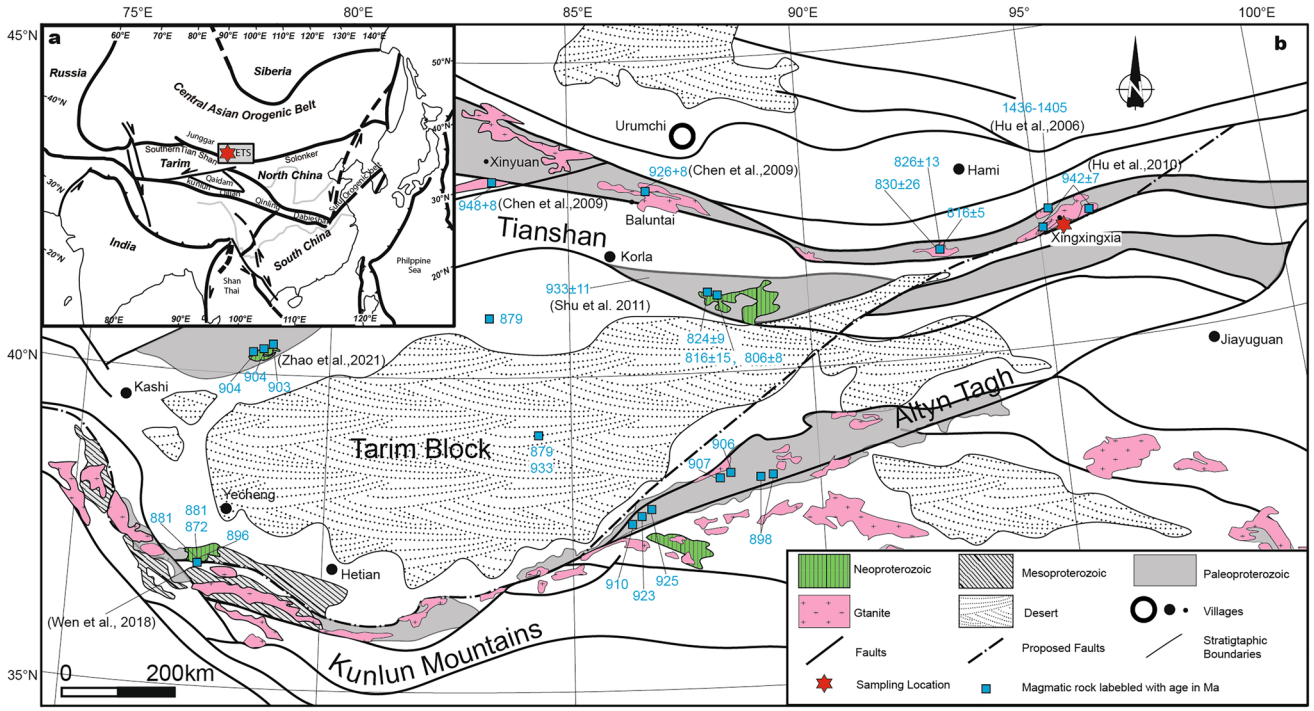

Fig. 1 **a** Simplified tectonic map of the Central Asian Orogenic Belt (CAOB: modified after (Jahn et al. 2000; Kröner et al. 2008; Şengör et al. 1993; Xiao and Santosh 2014). **b** Sketch map of the Tarim craton showing Precambrian geology and surrounding orogens, including the extensive Mesoproterozoic–Neoproterozoic (~1436–872 Ma) arc magmatism, the Eastern Tianshan and Beishan (modified after (He et al. 2019; Xiao and Santosh 2014; Xu et al. 2013; Zhao et al. 2021)

interspersed with terrigenous clastic rocks and partly rich in phosphorus, and represented by a suite of metamorphic rocks, mainly marbles, crystalline limestones, silicified limestones, wollastonite schists, and quartz schists (Chen 2006).

The gneissic granite in this study crops out in the south of the Xingxingxia town (E95°8′3.05441″, N41°46′57.28908″), displaying intrusive contacts with the Xingxingxia Group and fault contacts with the Jijitaizi mélange. The gneissic granite is medium- to coarse-grained in texture and gneissic in structure (Fig. 3a, b), with light layers composed of granular deformed and broken quartz and feldspar (Fig. 3c, d).

Analytical methods

Major elements were determined by X-ray fluorescence spectrometry (XRF), and trace elements by inductively coupled plasma techniques (ICP) at the Geological Test and Analysis Center of the Beijing Research Institute of Uranium Geology. Detailed procedures can be found in Mao et al. (2018).

The geochronological experiments on zircon U–Pb were adopted at Beijing Quick-Thermo Science & Technology Co., Ltd., using an ESI New Wave NWR 193UC (Two-Vol2) laser ablation system connected to an Agilent 8900 Inductively Coupled Plasma Mass Spectrometer (ICP-MS). The analytical procedures were followed Ji et al. (2020). The spot size and frequency of the laser were set to 20 μm and 5 Hz, respectively. Individual zircon grains (mounted and polished in epoxy) were ablated in a constant stream of He that is mixed downstream with N_2 and Ar before entering the torch region of the ICP–QQQ. After warmup of the ICP–QQQ and connection with the laser ablation system, the ICP-MS is first tuned for robust plasma conditions by optimizing laser and ICP–QQQ setting, monitoring $^{232}Th^{16}O^+/^{232}Th^+$ ratios (always ≤ 0.2%) and $^{238}U^+/^{232}Th^+$ ratios (always between 0.95 and 1.05) while ablating NIST SRM 610 in line scan mode. The 91,500 zircons were used as primary reference material for all U–Pb age determinations, while zircon PleŠovice was used as secondary reference. NIST610 glass was used to calibrate trace element with internal standard major element Si. The standards were analyzed two times before and after each analytical session including 6–8 spots on minerals. Background subtraction and correction for laser downhole elemental fractionation were performed using the Iolite data reduction package within the Wavemetrics Igor Pro data analysis software (Paton et al. 2011). Concordia plots were processed using ISOPLOT 4.15. Detailed operating conditions and data acquisition procedures were described by Ji et al. (2020).

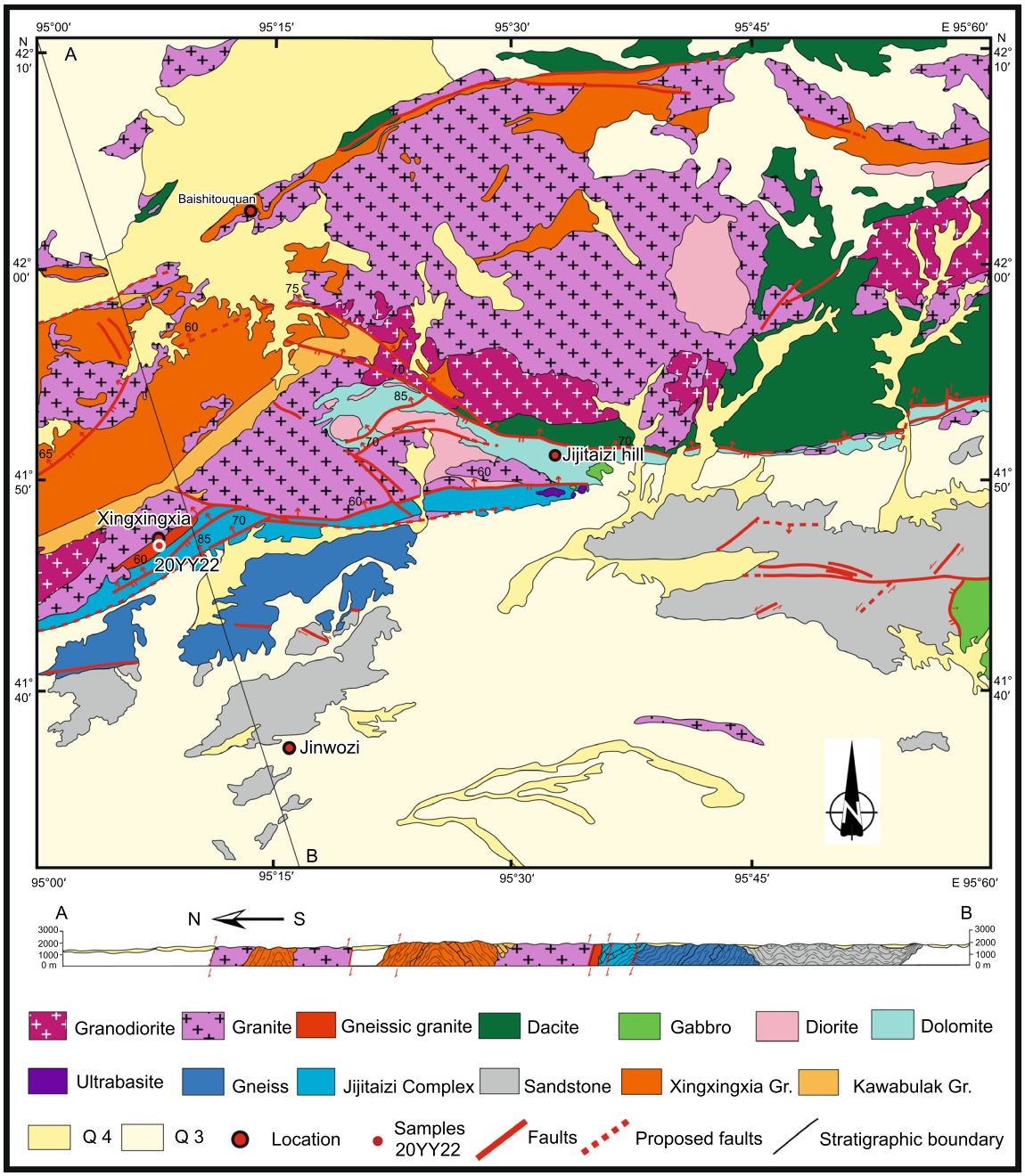

Fig. 2 The schematic geological map of Xingxingxia region in Eastern Tianshan (Mao et al. 2019; Xiao et al., 2004b) showing the locations of the gneissic granite

Zircon Lu–Hf in *situ* Lu–Hf isotope measurements were performed using a Thermo Finnigan Neptune-plus MC–ICP-MS fitted with a J-100 femto-second laser ablation system Applied Spectra Inc., housed at the Beijing Chron Technology Co., LTD, Beijing, China, which follow the analytical procedures and calibration methods are similar to those described by Wu et al. (2006). Zircons were ablated for 31 s at a repetition rate of 8 Hz at 16 J/cm^2, and ablation pits were ~ 30 μm in diameter. During analysis, the isobaric interference of 176Lu on 176Hf was negligible due to the extremely low $^{176}Lu/^{177}Hf$ in zircon (normally < 0.002). The mean $^{173}Yb/^{172}Yb$ value of individual spots was used to calculate the fractionation coefficient (β_{Yb}) and then to calculate the contribution of ^{176}Yb to ^{176}Hf. An isotopic ratio of $^{173}Yb/^{172}Yb = 1.35274$.

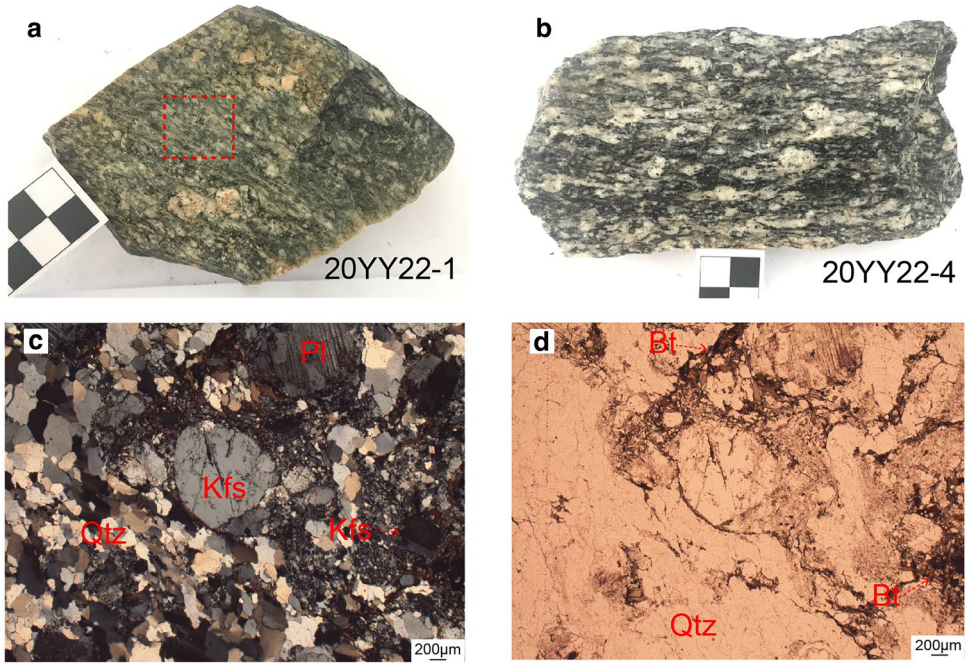

Fig. 3 Petrographic photos of the studied samples. **a** and **b** Close-ups of the Xingxingxia gneissic granite specimens; **c** photomicrograph of the representative sample 20YY22-1 (in cross-polarized light); **d** photomicrograph of the representative sample 20YY22-1 (in plane-polarized light). *Bt* biotite, *Pl* plagioclase, *Kfs* K-feldspar, *Qtz* quartz

Whole-rock geochemistry: major and trace elements

Eight samples from the gneissic granite are geochemically analyzed and the results are listed in Table 1.

The samples from the gneissic granite exhibit homogeneous geochemical characteristics, including high SiO_2 (70.66–73.92 wt.%), K_2O (2.80–3.93 wt.%), Na_2O (3.48–4.11 wt.%) and Al_2O_3 (14.07–15.09 wt.%), and low TiO_2 (0.19–0.28 wt.%), MgO (0.41–0.67 wt.%) and $^{T}Fe_2O_3$ (1.34–1.95 wt.%). They display high-K calc-alkaline features (Fig. 4a, b) and fall into the similar fields as the lower crust-derived adakitic rocks from the Cordillera Blanca batholith (Petford and Atherton 1996) and Kanguer accretionary complex (Mao et al. 2021a) in the K_2O–SiO_2 diagram. Their A/CNK values range from 1.02 to 1.08 (Fig. 4b), suggesting their weakly peraluminous affinities.

The samples have low Cr (6.64–12.93 ppm) and Ni (1.20–11.54 ppm), while their anomaly in Sr (202.6–343.4 ppm) and low Y (3.00–6.36 ppm) result in high Sr/Y ratios (47–114). In the primitive mantle-normalized multi-element patterns (Fig. 5a), the gneissic granite samples show obvious enrichment in Rb, Th, K, Pb, and Sr and depletion in Nb, Ta, P, and Ti, with slightly positive Zr–Hf anomalies. In the chondrite–normalized element rare earth element (REE) patterns, they are highly enriched in LREE($(La/Yb)_N = 7.64–9.86$), and show positive Eu anomalies ($Eu/Eu^* = 0.96–1.45$) (Fig. 5b).

Zircon U–Pb ages and in situ Lu–Hf isotopes

One gneissic granite sample (20YY22) was analyzed for zircon U–Pb ages and in situ Lu–Hf isotopic compositions. The analytical results are listed in Tables 2 and 3. The spot location for Lu–Hf isotopes was the same as that for zircon U–Pb analyses. Zircon grains separated from the gneissic granite are transparent, euhedral to subhedral and 80–100 μm long, with length/width ratios of 1:1 to 3:1.

Twelve zircons from the gneissic granite yielded unconcordant ages due to the Pb-loss. The remaining eight zircons have concordant ages and exhibit distinct oscillatory zoning with high Th/U ratios (0.47–0.93), consistent with a magmatic origin. They yielded $^{206}Pb/^{238}U$ ages of 856–889 Ma with a weighted mean age of 869 ± 9 Ma (MSWD = 2.5, 95% conf.) (Fig. 6a, b), suggesting that the gneissic granite emplaced in the Neoproterozoic.

Zircons from the gneissic granite possess similar Hf isotopic compositions, with $^{176}Hf/^{177}Hf$ ratios of 0.282232–0.282387 and positive $\varepsilon_{Hf}(t)$ values (+1.9 to +4.7) (Fig. 7; Table 3), indicating that the rock was mainly derived from the juvenile materials in the Paleo- to Mesoproterozoic Fig. 8.

Table 1 Major and trace elements of the Xingxingxia gneissic granite

Samples No	20YY22-2	20YY22-3	20YY22-4	20YY22-5	20YY22-6	XM01-1	XM01-2	XM01-3
SiO_2	72.25	71.30	73.92	70.66	71.72	71.92	71.54	72.68
TiO_2	0.21	0.27	0.19	0.28	0.23	0.26	0.27	0.24
Al_2O_3	14.76	15.09	14.07	15.59	15.05	14.86	15.02	14.41
$^{T}Fe_2O_3$	1.62	1.95	1.34	1.87	1.72	1.71	1.76	1.71
MnO	0.02	0.03	0.01	0.02	0.02	0.02	0.02	0.02
MgO	0.51	0.66	0.41	0.67	0.61	0.61	0.63	0.5
CaO	2.41	2.44	2.43	2.63	2.56	2.21	2.47	2.23
Na_2O	3.70	3.48	3.73	3.82	3.69	3.65	4.11	3.61
K_2O	3.57	3.58	2.80	3.11	3.30	3.93	3.17	3.71
P_2O_5	0.04	0.06	0.01	0.06	0.06	0.06	0.06	0.06
LOl	0.78	1.06	0.83	1.25	0.94	0.52	0.63	0.58
Sum	99.87	99.93	99.74	99.96	99.90	99.75	99.68	99.75
A/CNK	1.03	1.07	1.04	1.08	1.05	1.04	1.02	1.03
A/NK	1.48	1.57	1.54	1.61	1.56	1.45	1.47	1.45
Mg#	38.4	40.1	37.7	41.5	41.3	41.4	41.5	36.7
Li	14.47	14.00	9.13	13.08	12.43	15.51	17.80	15.53
Sc	2.33	2.85	2.15	2.56	4.08	4.19	4.37	4.20
V	17.84	23.04	14.21	23.00	22.72	16.80	16.98	14.22
Cr	9.59	12.93	6.64	11.53	12.39	9.43	9.96	8.05
Co	2.68	3.33	2.07	3.60	3.78	3.20	3.21	2.72
Ni	1.20	1.52	1.23	2.39	1.67	9.77	11.54	2.62
Cu	2.16	10.87	2.61	2.47	3.57	4.65	5.81	4.09
Zn	44.54	68.58	37.66	48.62	52.96	31.44	32.51	28.95
Ga	19.67	19.66	18.68	20.36	21.56	18.29	19.05	16.31
Rb	100.38	99.46	87.50	85.26	97.92	97.20	88.95	120.79
Sr	259.40	328.80	255.40	343.40	340.80	246.33	272.91	202.60
Y	3.51	3.83	3.52	3.55	3.00	4.61	5.20	6.36
Zr	166.42	197.40	173.96	187.40	190.88	148.93	162.13	133.47
Nb	3.77	4.88	3.90	5.01	4.37	6.34	6.22	5.38
Cs	2.10	2.57	3.25	3.52	1.96	2.37	2.60	5.07
Ba	641.20	954.00	558.00	976.40	865.40	771.98	642.30	982.71
La	24.06	31.16	25.44	25.90	33.22	29.59	30.51	28.85
Ce	41.68	56.74	43.76	43.92	60.60	50.12	45.54	47.14
Pr	3.90	5.05	4.06	4.16	5.18	4.89	4.93	4.63
Nd	12.71	16.56	12.93	13.59	16.79	15.41	15.21	14.24
Sm	1.90	2.36	1.76	1.92	2.32	2.59	2.53	2.38
Eu	0.59	0.77	0.54	0.78	0.74	0.68	0.67	0.68
Gd	1.31	1.57	1.14	1.32	1.50	1.83	1.778	1.72
Tb	0.14	0.16	0.12	0.14	0.14	0.20	0.21	0.22
Dy	0.68	0.72	0.60	0.68	0.59	0.84	0.92	1.10
Ho	0.12	0.13	0.11	0.12	0.10	0.13	0.15	0.20
Er	0.33	0.35	0.34	0.32	0.27	0.36	0.43	0.59
Tm	0.04	0.05	0.05	0.04	0.03	0.06	0.072	0.094
Yb	0.28	0.31	0.37	0.27	0.23	0.39	0.46	0.62
Lu	0.04	0.05	0.06	0.04	0.04	0.06	0.07	0.09
Hf	4.18	4.59	4.28	4.40	4.54	4.36	4.58	3.87
Ta	0.24	0.32	0.25	0.32	0.23	0.36	0.41	0.44
Pb	22.38	22.74	17.85	18.82	21.78	29.56	26.96	26.63
Th	7.91	8.73	9.63	7.93	9.33	11.88	14.43	9.31
U	0.98	1.13	1.15	0.89	1.21	1.31	1.69	1.09
Sr/Y	73.9	85.8	72.5	96.8	114	75.67	66.04	46.91

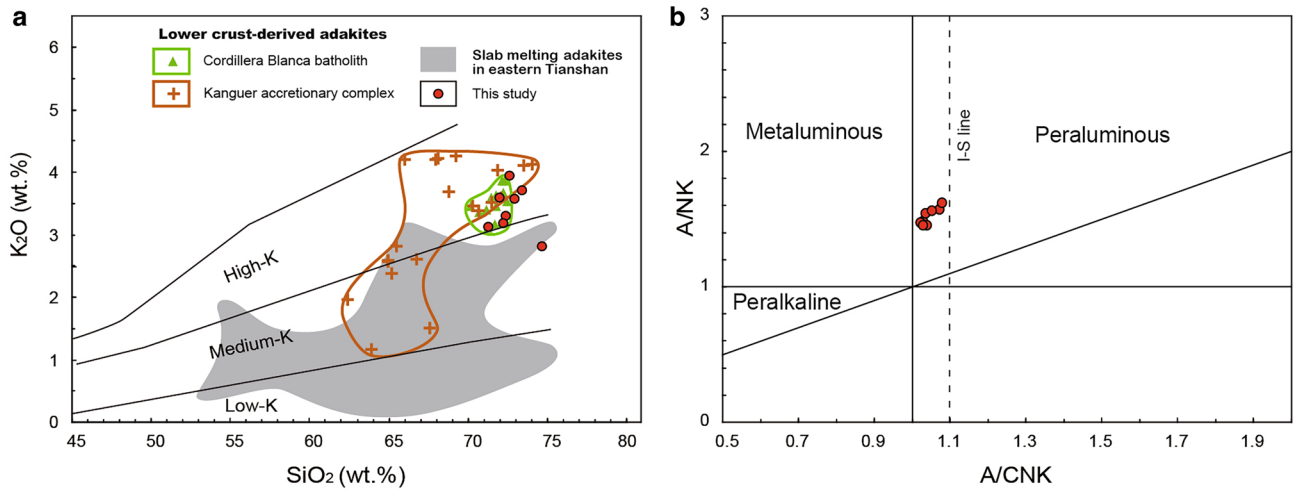

Fig. 4 **a** K_2O vs. SiO_2 diagram (Peccerillo and Taylor 1976); The adakitic intrusive rocks in this study show K_2O contents similar to those of the Cordillera Blanca batholith (Petford and Atherton 1996) and Kanguer accretionary complex (234–242.5 Ma) (Mao et al. 2021a, b), but higher than those of the slab-melted adakites in the Eastern Tianshan (Mao et al. 2019). **b** Al/(Na + K) vs. Al/(Ca + Na + K) diagram after (Maniar and Piccoli 1989)

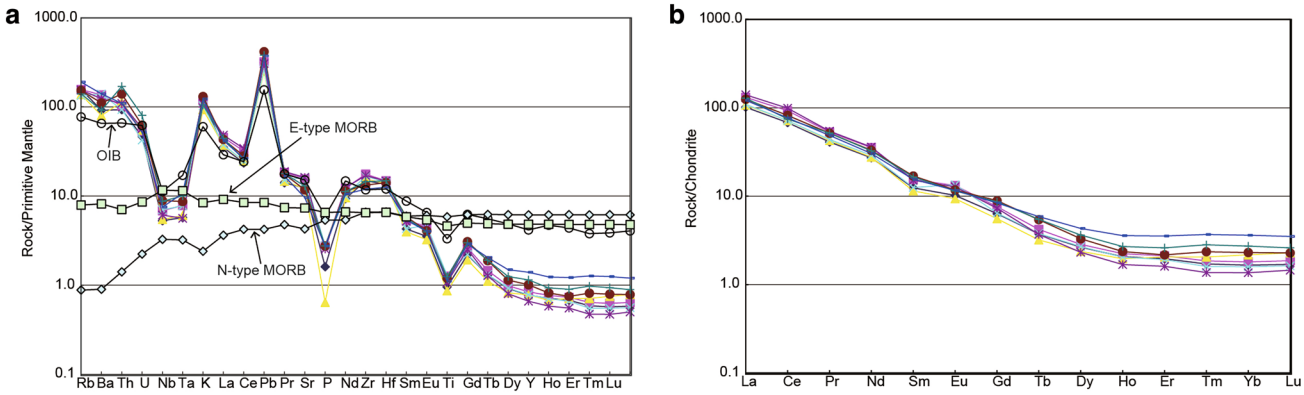

Fig. 5 $\varepsilon_{Hf}(t)$ **a** The primitive mantle-normalized multi-element diagrams and **b** the chondrite-normalized rare earth element (REE) patterns for the gneissic granite. The data for the N-type MORB, E-MORB and OIB are from Sun and McDonough (1989)

Discussion

Petrogenesis of the adakitic rocks

Adakites are a type of intermediate-acid magmatic rock with distinctive geochemical properties and significant geodynamic and metallogenetic implications (Wang et al. 2020). It is used to describe andesitic–rhyolitic extrusive to intrusive rocks having features including $SiO_2 \geq 56\%$, Na rich ($Na_2O \geq 3.5\%$), high Al ($Al_2O_3 \geq 15\%$) and Sr (> 400 ppm), low Y (≤ 18 ppm), strongly fractionated REE patterns (HREE depleted), positive Eu and/or Sr anomalies, as well as high Sr/Y and $(La/Yb)_N$ ratios (≥ 40 and 20, respectively). The Neoproterozoic Xingxingxia gneissic granite (869 ± 9 Ma) from the eastern Central Tianshan (NW China) contains high Sr/Y (47–114) and low levels of Y (3.00–6.36 ppm) and Yb (0.23–0.62 ppm), sharing strong geochemical similarities to adakitic rocks (Defant and Drummond 1990).

Adakites could form as a result of slab melting in a variety of modern subduction-arc settings, which may be related to subduction of young and hot oceanic crust (Calmus et al. 2003; Defant and Drummond 1990; Guivel et al. 1999; Wang et al. 2007; Yogodzinski et al. 1995), active ridge subduction (Aguillón-Robles et al. 2001; Bourgois and Michaud 2002; Johnston and Thorkelson 1997; Rogers et al. 1985; Reich et al. 2003; Thorkelson and Breitsprecher 2005), initiation of subduction (Sajona et al. 1993), flat subduction (Gutscher et al. 2000), and partial melting

Table 2 U–Pb isotopic data for multigrain analyses of zircons from gneissic granite

Samples No.	Isotope ratio						Age (Ma)					
	$^{207}Pb/^{235}U$	1δ	$^{206}Pb/^{238}U$	1δ	$^{207}Pb/^{206}U$	1δ	$^{207}Pb/^{235}U$	1δ	$^{206}Pb/^{238}U$	1δ	$^{207}Pb/^{206}U$	1δ
20YY22-2	1.503	0.067	0.1439	0.0038	0.0781	0.0021	929	27	866	21	1141	55
20YY22-6	1.385	0.028	0.1424	0.0029	0.0709	0.0011	884	13	858	16	949	33
20YY22-10	1.427	0.024	0.1467	0.0024	0.0695	0.0011	901	11	882	14	912	37
20YY22-13	1.385	0.028	0.142	0.0019	0.07072	0.00096	881	12	856	11	944	28
20YY22-14	1.397	0.028	0.1442	0.0022	0.0695	0.0012	887	12	868	12	905	36
20YY22-16	1.427	0.025	0.1449	0.0022	0.0715	0.0012	899	10	872	12	964	34
20YY22-17	1.464	0.03	0.1479	0.0028	0.0716	0.0013	914	12	889	16	967	37
20YY22-19	1.41	0.033	0.1449	0.0023	0.0696	0.0012	892	14	872	13	910	36
20YY22#1	1.383	0.024	0.1399	0.0016	0.0699	0.0012	881	10	843.9	9	919	37
20YY22#3	1.793	0.033	0.133	0.0019	0.0976	0.0016	1042	12	805	11	1572	31
20YY22#4	2.48	0.22	0.1104	0.0018	0.164	0.015	1239	65	675	11	2380	170
20YY22#5	2.01	0.11	0.1372	0.0015	0.1037	0.005	1110	37	828.8	8.8	1656	86
20YY22#7	2.115	0.031	0.1286	0.002	0.1174	0.002	1153	10	779	11	1910	31
20YY22#8	1.712	0.061	0.1412	0.0022	0.089	0.0032	1012	22	851	13	1374	67
20YY22#9	2.997	0.041	0.127	0.0028	0.1679	0.0048	1406	11	771	16	2527	50
20YY22#11	2.32	0.16	0.1391	0.0023	0.1224	0.0082	1208	49	839	13	1910	110
20YY22#12	2.62	0.19	0.1391	0.0038	0.142	0.011	1285	56	839	22	2160	140
20YY22#15	1.773	0.048	0.1396	0.0035	0.0913	0.0014	1034	18	842	19	1449	30
20YY22#18	2.851	0.095	0.1411	0.0029	0.1462	0.003	1363	25	850	16	2293	36
20YY22#20	1.494	0.034	0.151	0.0027	0.0716	0.0013	927	14	906	15	968	36

Table 3 Hf isotopic data for the zircons of the Xingxingxia gneissic granite

Sample No	$^{176}Hf/^{177}Hf$	2 δ	$^{176}Lu/^{177}Hf$	2 δ	$^{176}Yb/^{177}Hf$	2 δ	Age (Ma)	$\varepsilon_{Hf}(t)$	2 δ	$T_{DM1}(Hf)$
20YY22-2	0.282379	0.000013	0.000877	0.000019	0.027028	0.000570	869	4.7	0.5	1233
20YY22-6	0.282328	0.000018	0.000881	0.000010	0.023997	0.000364	869	2.9	0.6	1305
20YY22-10	0.282357	0.000013	0.000946	0.000007	0.028124	0.000320	869	3.9	0.5	1266
20YY22-13	0.282321	0.000017	0.000969	0.000005	0.026510	0.000188	869	2.6	0.6	1318
20YY22-14	0.282344	0.000017	0.001078	0.000027	0.030087	0.000901	869	3.4	0.6	1289
20YY22-16	0.282302	0.000016	0.001055	0.000007	0.028573	0.000283	869	1.9	0.6	1348
20YY22-17	0.282316	0.000015	0.000839	0.000005	0.022816	0.000143	869	2.5	0.5	1320
20YY22-19	0.282303	0.000016	0.000851	0.000010	0.023692	0.000382	869	2.0	0.6	1339

of lower crust of thickened arc (Defant 2002; Petford and Atherton 1996). However, several other mechanisms were also proposed for their generation, such as the differentiation of mantle-derived basaltic magmas (Castillo et al. 1999; Macpherson et al. 2006), magma mixing (Chen et al. 2013), and partial melting of lower crustal, hydrated mafic rocks in magmatically or tectonically thickened crust or partial melting of delaminated lower crust (Atherton and Petford 1993; Jiang et al. 2012; Kay and Kay 2002; Kay and Mpodozis 2002; Kay et al. 1993; Muir et al. 1995; Peacock et al. 1994; Windley et al. 2010; Xiong et al. 2001; Zhang et al. 2002; Zhao et al. 2006).

The Xingxingxia gneissic granite contains high SiO_2 (> 70 wt.%) and low MgO (< 0.7 wt.%) contents, as well as a narrow range of major and trace element compositions (Table 1). Additionally, the pluton lacks a mafic endmember and contemporaneous mafic rocks are absent in the study area, implying hypotheses of fractional crystallization of mantle-derived magmas or mixing of mantle- and crust-derived magmas inadequately account for its genesis.

Furthermore, the low Mg# (37–42), Cr (6.64–12.93 ppm) and Ni (1.20–11.54 ppm) contents of the Xingxingxia gneissic granite are also inconsistent with their derivation by slab melting. The gneissic granite has relatively high K_2O contents, which is comparable to those of the adakitic rocks derived from the thickened lower curst of the Andes arc in the Peru (Petford and Atherton

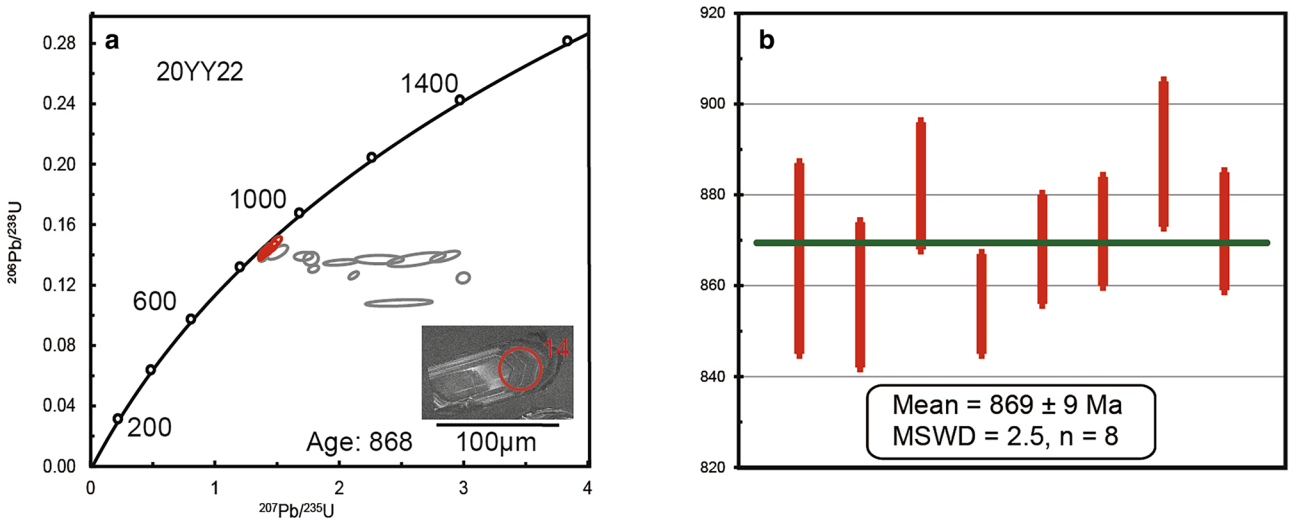

Fig. 6 **a** K_2O vs. SiO_2 (Peccerillo and Taylor 1976); K_2O (Petford and Atherton 1996) (Mao et al. 2021a, b), (Mao et al. 2019). **b** Al/(Na + K) vs. Al/(Ca + Na + K) (Maniar and Piccoli 1989) a Zircon representative CL image and U–Pb Concordia diagram and b age histogram of the Xingxingxia gneissic granite

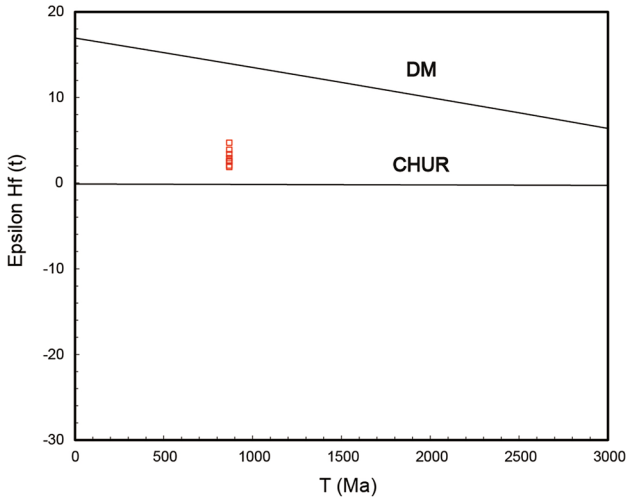

Fig. 7 Diagram of zircon εHf(t) versus age (1989)

1996) and the Dananhu arc (Mao et al. 2021a) (Figs. 4a and 9a) but higher than the slab-derived adakites in the Eastern Tianshan (Mao et al. 2021a, b) (Fig. 4a). In combination with its moderate positive Hf isotopic compositions, we suggest that the gneissic granite formed as a result of partial melting of juvenile lower crust of the eastern Central Tianshan arc. The very low HREE and relatively low CaO, $^{T}Fe_2O_3$ and Al_2O_3 contents of the Xingxingxia gneissic granite further imply that it was produced from thickened lower crust (Yang et al. 2020). In the Rb vs. Y + Nb diagram, the Xingxingxia gneissic granite plots in the field of volcanic granites (Fig. 9b).

Implications for long-lived subduction and crustal growth

To better constrain the source and tectonic setting of the Xingxingxia adakitic rock, it is necessary to compare it with those from other orogens where the similar thickened lower crust-derived adakitic rocks were reported (Fig. 10), such as the Early Cretaceous adakitic rocks in Eastern China that were derived from thickened or delaminated lower crust (Wang et al. 2004; Xu et al. 2002). Our adakitic rock tends to be more depleted in isotopes than those adakitic rocks formed in intra-continental or collisional settings in which the orogen experienced tectonically thickening or lower-crustal delamination.

As another lower-crustal melting example, the Late Miocene Cordillera Blanca batholith adakitic rocks in Peru were generated by the thickened Andean arc (Petford and Atherton 1996) and the magmas formed by partial melting of newly underplated materials that were quickly melted following the formation of underplate to produce the Cordillera Blanca Na-rich suite (Petford and Atherton 1996). This case for the generation of adakitic rocks, indeed, reflects the process of continental crustal growth. The Xingxingxia gneissic granite geochemically comparable to the adakitic rocks of the Cordillera Blanca batholith (Fig. 4a), and it has relatively depleted Hf isotopic composition (Fig. 7), representing the product of subduction-crustal growth during the Neoproterozoic.

The geochemical properties of the Xingxingxia gneissic granite, which include enrichment of LILE and LREE and depletion of HFSE and HREE with evidently negative Nb

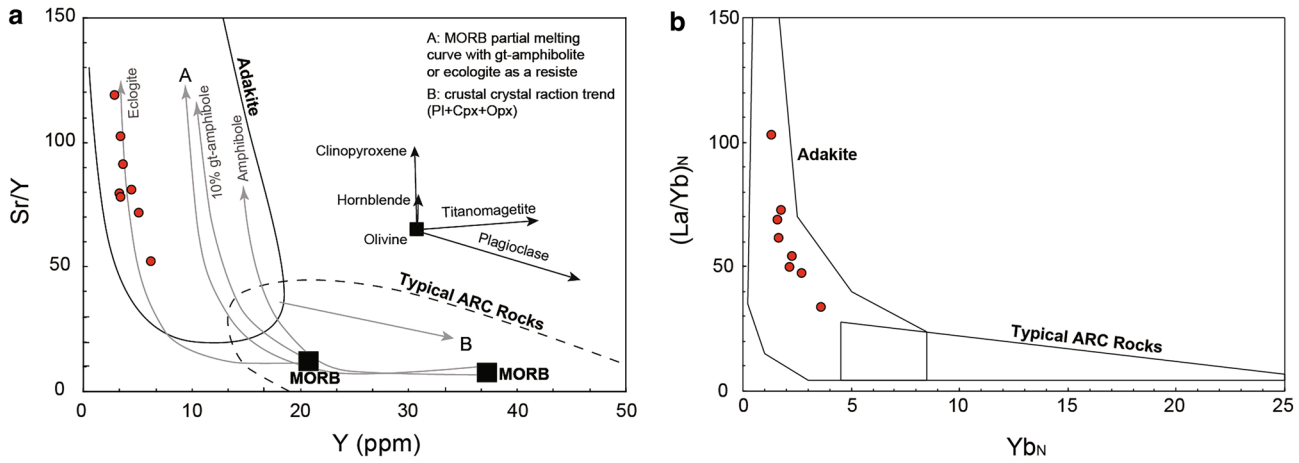

Fig. 8 **a** Sr/Y vs. Y diagram. The fields for adakites and classical island arc magmatic rocks are from (Defant and Drummond 1990); **b** $(La/Yb)_N$ vs Yb_N diagram. The fields for the adakites and classical island arc magmatic rocks are from Martin (1999)

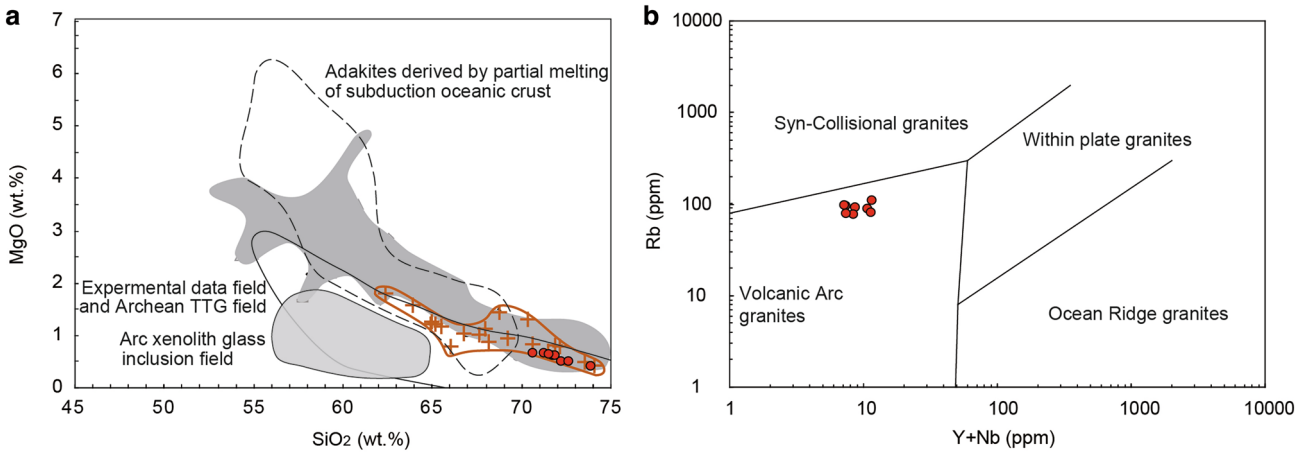

Fig. 9 **a** MgO vs. SiO_2 diagram for the adakitic rocks and experimental basaltic partial melts. Data sources and legends are the same as in Fig. 5a; **b** Discrimination diagram of tectonic setting for the Xingxingxia gneissic granite. Symbols are the same as those in Fig. 4

and Ta anomalies, are consistent with those of magma in an island arc setting (Fig. 5).

Therefore, the southern PAO had its accretionary tectonic history that may have been extended into the Neoproterozoic. Our newly found adakitic rocks indicate that the PAO may have evolved into a mature stage at ca. 870 Ma along the Central Tianshan Arc. This is consistent with previous studies suggesting that the PAO may have begun at least ~ 1020 Ma ago (Rytsk et al. 2007; Gordienko et al. 2009; Kuzmichev et al. 2005).

It is well known that the PAO generally became younger southward, and in the Late Paleozoic PAO had several branches in the southern Altaids, including the ones around the Central Tianshan Arc (Şengör et al. 1993; Windley et al. 2007; Xiao et al. 2015a, b). Our work, together with some previous data, shows that the branches around the Central Tianshan Arc had a long evolutionary history at least from ca. 870 Ma lasting to the Late Paleozoic and even Triassic (Chen et al. 2019; Ao et al. 2021; Mao et al. 2021a). Actually, other PAO branches north to the Tianshan, such as the Erqis and other sutures in the Junggar and adjacent areas may have been closed earlier (Wang et al. 2012; Xiao et al. 2015a; Li et al. 2015; Yang et al. 2015; Song et al. 2020; Guy et al. 2020). Therefore, the oceanic slabs beneath the Central Tianshan arc could have represented one of the major ocean(s) of the PAO with long-lived subduction-related accretion, which generated a substantial foundation for considerable Phanerozoic continental growth (Şengör et al. 1993; Windley et al. 2007; Xiao et al. 2015a, 2018).

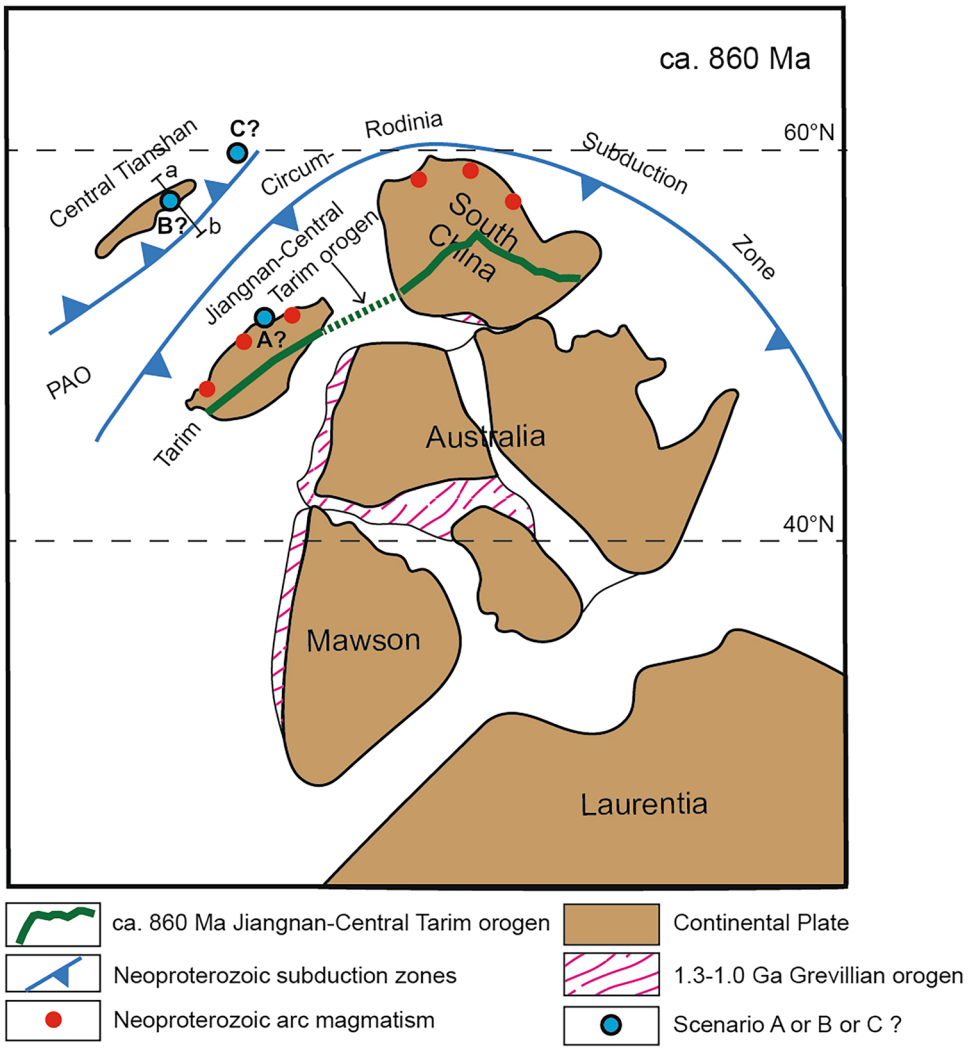

Fig. 10 Paleogeographic reconstructions of the northern Rodinia at ca. 860 Ma after (Zhao et al. 2021). The reconstructions are based on the paleolatitude of each block also accounting for geological evidence. Final closure of Jiangnan–Central Tarim Ocean, approaching amalgamation of the South China and Tarim, and the (relative) paleogeographic position the Central Tianshan separated from the Tarim and South China by the Circum–Rodinia Subduction Zone were reconstructed between ~ 870 and 820 Ma. This map is in Mollweide projection

Tectonic scenarios and implications for northern Rodinia reconstruction

Based on the identification of 1.4–0.9 Ga high grade metamorphism (Hu et al. 2006, 2010; Spencer et al. 2017) and paleomagnetic reconstructions (Evans 2013; Li et al. 2008a; Wen et al. 2018), the configuration of the earliest Rodinia orogenesis could be the reconstruction of the Umkondo large igneous province with the aggregated of Kalahari, Amazonia, Congo, and other cratons of the southern Rodinia by the time of ca. 1.1 Ga, which has been referred to as "Umkondia" (Choudhary et al. 2019). Additionally, during the Grenvillian orogenesis (1.3–1.0 Ga), the core of Rodinia was rebuilt with the assembly of Australia–East Antarctica, Amazonia (of Umkondia), and Baltica, which were located along the western, eastern, and northeastern margins of the Laurentia, respectively (Hoffman 1999; Li et al. 2008a).

Even the Cathaysia and South Tarim, potentially adjacent or connected to each other, likely joined Rodinia to the north of Australia in the early Neoproterozoic. The Central Tianshan, South China and Tarim had not yet amalgamated as discrete cratons (Cawood et al. 2013; Wen et al. 2018). The evidence for the subduction of the Jiangnan–Central Tarim Ocean is found in the Neoproterozoic arc magmatism along multiple active margins of Yangtze, Cathaysia, and North Tarim, demonstrating that the Beishan, as a part of the Central Tianshan, is still separated from Tarim and South China by the Circum–Rodinia subduction zone after the closure of the Jiangnan–Central Tarim Ocean between 870 and 820 Ma (Fig. 10) (Yao et al. 2019; Zhao et al. 2011).

The Eastern Tianshan consists of multiple arcs, accretionary complex belts and microcontinental blocks and is crucial for understanding the earlier accretionary and collisional processes of the southern Altaids (Muhtar et al. 2020; Wang et al. 2014a; Xiao et al. 2015a). The polarity of this subduction zone or whether two-sided subduction was developed remain unresolved due to the scarcity of evidence for the Central Tarim suture. There are several competing models for the collision between Yangtze and Cathaysia, ranging from northwestward subduction beneath the Yangtze (Yan

et al. 2019; Zhao et al. 2011) to southeastward subduction beneath the Cathaysia (Cawood et al. 2013; Yao et al. 2019) to two-sided subduction beneath both Yangtze and Cathaysia (Zhao 2015). In any case, there is evidence following peripheral accretion of the Yangtze and North Tarim, a circum–Rodinia subduction girdle with arc magmatism developed along the external margins of the South China, Tarim, and Australia (Cawood et al. 2018) (Fig. 10).

While the Eastern Tianshan includes several microcontinents or arcs with Precambrian basement, the adakite may suggest that its tectonic affinity was proposed as the following three main scenarios (A, B and C) in view of the complicated evolutionary histories of the Rodinia and Gondwana. They are the three potential kinematic solutions for the final assembly of Rodinia along its northern margin.

In scenario A (Andean-type arc), the adakite was intruded into the magmatic arc or back-arc position of the northern Tarim carton. This occurred as the consequence of retreating subduction in the North Tarim block at ca. 730 Ma, with the opening of the Proto Tethys Ocean and South and North Altyn Oceans resulted by the breakup of the Rodinia (Ma et al. 1997; Wang et al. 2022) (Fig. 10).

In scenario B, there was a Japan-type arc composed of subduction-related rocks mostly on an oceanic plate with some recycled materials in the PAO (Fig. 10).

In scenario C (Mariana-type arc), the subduction also possibly occurred in an intra-oceanic setting in the vast PAO like what happens today along the Mariana subduction zone in the western Pacific Ocean, developing juvenile magmatic arcs in an oceanic plate (e.g., Yao et al. 2021).

Subduction zone develops various types of island arc system, including the Andean type, Japan type, Mariana type, and Alaska type, depending on the attributes of the upper plate in subduction system (Xiao et al. 2010). The Andean type, Japan type, and Mariana type can be listed as the scenarios A, B and C, respectively. The Alaska type is taken from the northern North American craton where the Alaska extends to connect the Aleutian arc south to the Bering Sea, which is a representative kind of mixture type of the Andean type, Japan type, and Mariana type.

Based on the chemical characteristics, such as obvious negative anomalies in Nb, Ta and Ti elements, and Hf and Nd isotopic compositions, all the Xingxingxia granitoids in 1.4 Ga and 0.9 Ga from the Western and Eastern Tianshan were suggested to be generated in a continental margin tectonic setting and formed by remelting of Paleoproterozoic rocks, followed by advanced fractional crystallization, probably forming a part of the Rodina during the early Neoproterozoic period (Hu et al. 2006, 2010).

The Hf isotopes in this study show relatively lower positive $\varepsilon_{Hf}(t)$ signature, contrasting to an intro-oceanic subduction-arc system like Mariana type, which contains highly positive $\varepsilon_{Hf}(t)$ feature close to juvenile or depleted mantle source. The northern margin of the Precambrian Tarim carton, on the contrary, shows dominantly negative $\varepsilon_{Hf}(t)$ and $\varepsilon_{Nd}(t)$ isotopic feature due to incorporating large amounts of reworked crustal material in an Andean-type subduction (Ge et al. 2014; He et al. 2013; Long et al. 2015; Zhang et al. 2007a), e.g., the lower crust-derived adakitic granites (795–820 Ma) in the northeastern Tarim have the εNd(t) values varying from −12.7 to −17.3 (Zhang et al. 2007a). Given the fact that the Central Tianshan was constructed by newly deformed arcs, accretionary complexes and ancient microcontinental blocks, juvenile and reworking (remelting) material could serve as the source for the composite isotopic compositions and result in a relative (intermediate) positive $\varepsilon_{Hf}(t)$ feature (Hu et al. 2000). Therefore, we exclude scenario A and favor scenario B in which the arc on which our adakite was mostly a Japan-type one. Of course, it may also have been an Alaska type.

On the basis of the foregoing facts and arguments, we can postulate that, when the adakitic rock of this study was

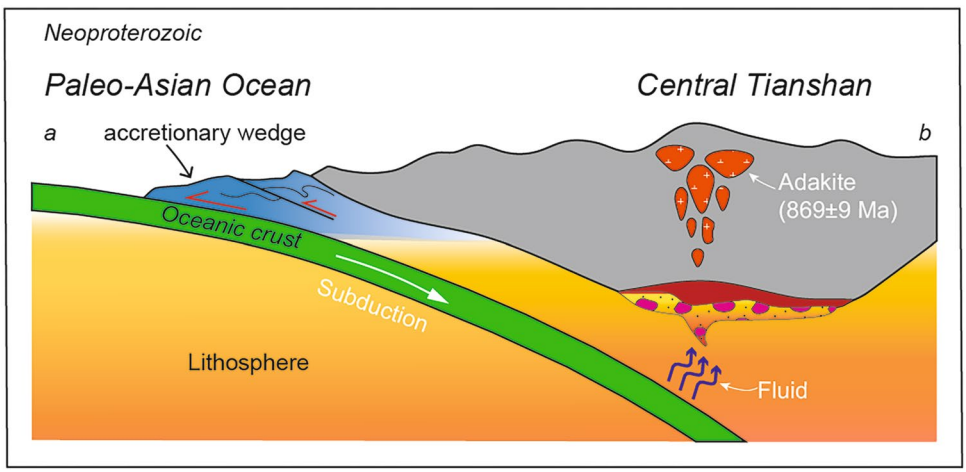

Fig. 11 Schematic tectonic model for the evolution of the adakites in the Xingxingxia area, eastern Tianshan (modified after Mao et al. (2012))

intruded at ca. 869 ± 9 Ma, the Central Tianshan arc had not yet amalgamated with the Tarim block to the south (Fig. 10), which had relatively juvenile crust in the Neoproterozoic. On the other hand, the Eastern Tianshan as a peripheral island arc in the PAO developed to the north of the Yangtze and North Tarim, was assembled along the northern margin of the Rodinia, heralding the long-lived of arcs in the PAO following the final amalgamation of the Neoproterozoic supercontinent.

Our work suggests that there was an arc in this part of the PAO as a Japan type or as an Alaska type. Therefore, the arc growth in the Xingxingxia area was most possibly taken root in the Central Tianshan, indicating that the subduction of the PAO might have taken place in the Neoproterozoic (Fig. 11).

Conclusions

(1) Our new zircon U–Pb dating reveals that the Xingxingxia gneissic granite from the eastern Central Tianshan (NW China) was formed in the Neoproterozoic (869 ± 9 Ma).
(2) The geochemical data indicate that the Xingxingxia gneissic granite has high Sr/Y, low Y and Yb and strongly fractionated REE patterns, indicating an adakitic affinity. It was derived from thickened juvenile arc lower crust and represents the products of Neoproterozoic subduction and corresponding continental crustal growth.
(3) The subduction of the Paleo-Asian oceanic slab beneath the Central Tianshan occur at least in the Neoproterozoic, which resulted in the crustal thickening and melting of the thickened crust. Therefore, it is a solid and key evidence to show that the tectonic position of the major Paleo-Asian Ocean was located in the South/North Tianshan, where the paleo-oceanic basin evolved into its mature stage with the subduction beneath the Central Tianshan at ca. 870 Ma.
(4) Our work also sheds light on the reconstruction of the Rodinia and the interaction of the Paleo-Asian Ocean with the Jiangnan–North Tarim Ocean.

Acknowledgements We appreciate the Editors and reviewers, Yunpeng Dong and an anonymous one, for their constructive comments and suggestions that substantially improved the presentation of our work. This study was financially supported by the Third Xinjiang Scientific Expedition Program (2022xjkk1301), the National Natural Science Foundation of China (41888101, 41822204), One Hundred Talent Program of the Chinese Academy of Sciences (CAS), the Science and Technology Major Project of Xinjiang Uygur Autonomous Region, China (2021A03001-1 & 4), the National Key Research and Development Program of China (2017YFC0601201), Youth Innovation Promotion Association Chinese Academy of sciences (2022446), the Chinese Ministry of Land and Resources for the Public Welfare Industry Research (201411026-1), the "Light of West China" Program of the CAS (2017-XBQNXZ-B-013, 2018-XBYJRC-003), and a Project of the China-Pakistan Joint Research Center on Earth Sciences of the CAS (131551KYSB20200021). This is a contribution to IGCP 622 and IGCP 710.

Data availability All data generated or analyzed during this study are included in this article.

References

Aguillón-Robles A, Calmus T, Benoit M, Bellon H, Maury RC, Cotten J, Bourgois J, Michaud F (2001) Late Miocene adakites and Nb-enriched basalts from Vizcaino Peninsula, Mexico: indicators of East Pacific rise subduction below southern Baja California? Geology 29(6):531–534

Ao S, Mao Q, Windley BF, Song D, Zhang Z, Je Z, Wan B, Han C, Xiao W (2021) The youngest matrix of 234 Ma of the Kanguer accretionary mélange containing blocks of N-MORB basalts: constraints on the northward subduction of the Paleo-Asian Kanguer Ocean in the Eastern Tianshan of the Southern Altaids. Int J Earth Sci 110(3):791–808

Atherton MP, Petford N (1993) Generation of sodium-rich magmas from newly underplated basaltic crust. Nature 362(6416):144–146

Berzin NA, Dobretsov NL (1994) Geodynamic evolution of southern Siberia in late Precambrian-early Paleozoic time. Reconstruction of the Paleo-Asian Ocean: 45–62

Bourgois J, Michaud F (2002) Comparison between the Chile and Mexico triple junction areas substantiates slab window development beneath northwestern Mexico during the past 12–10 Myr. Earth Planet Sci Lett 201(1):35–44

Calmus T, Aguillón-Robles A, Maury R, Bellon H, Benoit M, Cotten J, Bourgois J, Michaud F (2003) Spatial and temporal evolution of basalts and magnesian andesites ("bajaites") from Baja California, Mexico: the role of slab melts. Lithos 66(1–2):77–105

Castillo PR, Janney PE, Solidum RU (1999) Petrology and geochemistry of Camiguin Island, southern Philippines: insights to the source of adakites and other lavas in a complex arc setting. Contrib Mineral Petrol 134(1):33–51

Cawood PA, Wang Y, Xu Y, Zhao G (2013) Locating South China in Rodinia and Gondwana: A fragment of greater India lithosphere? Geology 41(8):903–906

Cawood PA, Zhao G, Yao J, Wang W, Xu Y, Wang Y (2018) Reconstructing South China in phanerozoic and precambrian supercontinents. Earth Sci Rev 186:173–194

Charvet J, Shu L, Laurent-Charvet S, Wang B, Faure M, Cluzel D, Chen Y, De Jong K (2011) Palaeozoic tectonic evolution of the Tianshan belt. NW China Sci China Earth Sci 54(2):166–184

Chen Y (2006) Geological characteristics and ore genesis of the Xiaobaishitou tungsten (–molybdenum) deposit, Xinjiang. Gansu Metall 28:75–81 (**(in Chinese with English abstract)**)

Chen G, Pei X, RuiBao L, ZuoChen L, PeiI L, Liu Z, Chen Y, Liu C (2013) Late Triassic magma mixing in the East Kunlun orogenic belt: A case study of Helegang Xilikete granodiorites. Geol China 40(4):1044–1065

Chen Z, Xiao W, Windley BF, Schulmann K, Mao Q, Zhang Z, Zhang J, Deng C, Song S (2019) Composition, provenance, and tectonic setting of the southern Kangurtag accretionary complex in the Eastern Tianshan, NW China: Implications for the late Paleozoic evolution of the North Tianshan Ocean. Tectonics 38(8):2779–2802

Choudhary BR, Ernst RE, Xu Y, Evans DA, de Kock MO, Meert JG, Ruiz AS, Lima GA (2019) Geochemical characterization of a reconstructed 1110 Ma large igneous province. Precambr Res 332:105382

Coney PJ (1992) The Lachlan belt of eastern Australia and circum-Pacific tectonic evolution. Tectonophysics 214(1–4):1–25

Defant M (2002) Adakites: some variations on a theme. Acta Petrologica Sinica 18:129–142

Defant MJ, Drummond MS (1990) Derivation of some modern arc magmas by melting of young subducted lithosphere. Nature 347(6294):662–665

Deng X, Chen Y, Santosh M, Wang J, Li C, Yue S, Zheng Z, Chen H, Tang H, Dong L (2017) U-Pb zircon, Re–Os molybdenite geochronology and Rb–Sr geochemistry from the Xiaobaishitou W (–Mo) deposit: implications for Triassic tectonic setting in eastern Tianshan, NW China. Ore Geol Rev 80:332–351

Dobretsov NL, Buslov MM, Vernikovsky VA (2003) Neoproterozoic to Early Ordovician evolution of the Paleo-Asian Ocean: implications to the break-up of Rodinia. Gondwana Res 6(2):143–159

Evans DA (2013) Reconstructing pre-Pangean supercontinents. GSA. Bulletin 125(11–12):1735–1751

Gao Z, Chen J, Lu S, Peng C, Qin Z (1993) Precambrian system of the Northern Xinjiang. Geol Publ House, Beijing: 1–153 **(in Chinese with English abstract)**

Ge R, Zhu W, Wilde SA, He J, Cui X, Wang X, Bihai Z (2014) Neoproterozoic to Paleozoic long-lived accretionary orogeny in the northern Tarim Craton. Tectonics 33(3):302–329

Gordienko I, Bulgatov A, Lastochkin N, Sitnikova V (2009) Composition and U-Pb isotopic age determinations (SHRIMP II) of the ophiolitic assemblage from the Shaman paleospreading zone and the conditions of its formation (North Transbaikalia). In: Doklady Earth Sciences, vol 429. Springer, pp 1420–1425

Gu L (2006) Some problems on granites and vertical growth of the continental crust in the eastern Tianshan Mountains, NW China. Acta Petrologica Sinica 22(5):1103–1120 ((**in Chinese with English abstract**))

Gu L, Hu S, Chu Q, Yu C, Xiao X (1999) Pre-collision granites and post-collision intrusive assemblage of the Kelameili-Harlik orogenic belt. Acta Geologica Sinica (english Edition) 73(3):316–329

Guivel C, Lagabrielle Y, Bourgois J, Maury R, Fourcade S, Martin H, Arnaud N (1999) New geochemical constraints for the origin of ridge-subduction-related plutonic and volcanic suites from the Chile Triple Junction (Taitao Peninsula and Site 862, LEG ODP141 on the Taitao Ridge). Tectonophysics 311(1–4):83–111

Guo Z, Li M (1993) On the Early Paleozoic dispersed terranes in mid-Tianshan. Acta Scicentiarum Naturalum Universitis Pekinesis 29(3):356–362 ((**in Chinese with English abstract**))

Gutscher MA, Spakman W, Bijwaard H, Engdahl ER (2000) Geodynamics of flat subduction: Seismicity and tomographic constraints from the Andean margin. Tectonics 19(5):814–833

Guy A, Schulmann K, Soejono I, Xiao W (2020) Revision of the Chinese Altai-east Junggar terrane accretion model based on geophysical and geological constraints. Tectonics 39(4): e2019TC006026.

Hastie AR, Cox S, Kerr AC (2021) Northeast-or southwest-dipping subduction in the Cretaceous Caribbean gateway? Lithos 386:105998

He Z, Zhang Z, Zong K, Dong X (2013) Paleoproterozoic crustal evolution of the Tarim Craton: constrained by zircon U-Pb and Hf isotopes of meta-igneous rocks from Korla and Dunhuang. J Asian Earth Sci 78:54–70

He Z, Klemd R, Yan L, Lu T, Zhang Z (2018) Mesoproterozoic juvenile crust in microcontinents of the Central Asian Orogenic Belt: evidence from oxygen and hafnium isotopes in zircon. Sci Rep-Uk 8(1):1–7

He J, Xu B, Li D (2019) Newly discovered early Neoproterozoic (ca. 900 Ma) andesitic rocks in the northwestern Tarim Craton: Implications for the reconstruction of the Rodinia supercontinent. Precambr Res 325:55–68

Hoffman PF (1999) The break-up of Rodinia, birth of Gondwana, true polar wander and the snowball Earth. J Afr Earth Sc 28(1):17–33

Hu A, Jahn B, Zhang G, Chen Y, Zhang Q (2000) Crustal evolution and Phanerozoic crustal growth in northern Xinjiang: Nd isotopic evidence. Part I. Isotopic characterization of basement rocks. Tectonophysics 328(1–2):15–51

Hu A, Wei G, Deng W, Chen L (2006) SHRIMP zircon U-Pb dating and its significance for gneisses from the southwest area to Qinghe County in the Altai. China Acta Petrologica Sinica 22(1):1–10 ((**in Chinese with English abstract**))

Hu A, Wei G, Zhang J, Deng W, Chen L (2007) SHRIMP U-Pb age for zircons of East Tianhu granitic gneiss and tectonic evolution significance from the eastern Tianshan Mountains, Xinjiang. China Acta Petrologica Sinica 23(8):1795–1802

Hu A, Wei G, Jahn B, Zhang J, Deng W, Chen L (2010) Formation of the 0.9 Ga Neoproterozoic granitoids in the Tianshan Orogen, NW China: constraints from the SHRIMP zircon age determination and its tectonic significance. Geochimica et Cosmochimica Acta 39(3):197–212

Jahn B, Wu F, Chen B (2000) Massive granitoid generation in Central Asia: Nd isotope evidence and implication for continental growth in the Phanerozoic. Episodes 23(2):82–92

Ji W, Wu F, Wang J, Liu X, Liu Z, Zhang Z, Cao W, Wang J, Zhang C (2020) Early evolution of Himalayan Orogenic Belt and generation of middle Eocene magmatism: Constraint from Haweng granodiorite porphyry in the Tethyan Himalaya. Front Earth Sci 8:236

Jiang W, Zhang J, Tian T, Wang X (2012) Crustal structure of Chuan-Dian region derived from gravity data and its tectonic implications. Phys Earth Planet Inter 212:76–87

Johnston ST, Thorkelson DJ (1997) Cocos-Nazca slab window beneath central America. Earth Planet Sci Lett 146(3–4):465–474

Kay RW, Kay SM (2002) Andean adakites: three ways to make them. Acta Petrologica Sinica 18(3):303–311

Kay SM, Mpodozis C (2002) Magmatism as a probe to the Neogene shallowing of the Nazca plate beneath the modern Chilean flat-slab. J S Am Earth Sci 15(1):39–57

Kay SM, Ramos V, Marquez M (1993) Evidence in Cerro Pampa volcanic rocks for slab-melting prior to ridge-trench collision in southern South America. J Geol 101(6):703–714

Khain VE, Bozhko NA (1988) Historical Geotectonics: The Precambrian. Moscow Izdatel Nedra

Khain E, Bibikova E, Salnikova E, Kröner A, Gibsher A, Didenko A, Degtyarev K, Fedotova A (2003) The Palaeo-Asian ocean in the Neoproterozoic and early Palaeozoic: New geochronologic data and palaeotectonic reconstructions. Precambr Res 122(1–4):329–358

Kröner A, Hegner E, Lehmann B, Heinhorst J, Wingate M, Liu D, Ermelov P (2008) Palaeozoic arc magmatism in the Central Asian Orogenic Belt of Kazakhstan: SHRIMP zircon ages and whole-rock Nd isotopic systematics. J Asian Earth Sci 32(2–4):118–130

Kuzmichev A, Kröner A, Hegner E, Dunyi L, Yusheng W (2005) The Shishkhid ophiolite, northern Mongolia: a key to the reconstruction of a Neoproterozoic island-arc system in central Asia. Precambr Res 138(1–2):125–150

Li J, Kusky TM (2007) World's largest known Precambrian fossil black smoker chimneys and associated microbial vent communities, North China: Implications for early life. Gondwana Res 12(1–2):84–100

Li X, Zhang L, Wei C, Ai Y, Chen J (2007) Petrology of rodingite derived from eclogite in western Tianshan. China J Metamorphic Geol 25(3):363–382

Li Z, Bogdanova S, Collins A, Davidson A, De Waele B, Ernst R, Fitzsimons I, Fuck R, Gladkochub D, Jacobs J (2008a) Assembly, configuration, and break-up history of Rodinia: a synthesis. Precambr Res 160(1–2):179–210

Li Z, Zhu X, Tang S, Li Y (2008b) Fe isotope fractionation between magnetite and pyrite during green schist-lower amphibolites facies metamorphism. Acta Petrologica Et Mineralogica 27(4):291–297

Li D, He D, Santosh M, Ma D, Tang J (2015) Tectonic framework of the northern Junggar Basin part I: The eastern Luliang Uplift and its link with the East Junggar terrane. Gondwana Res 27(3):1089–1109

Liu X, Wang Q (1995) Geotectonics and its evolution of the Beishan orogenic belts in the northwestern China. Geosci Res 28:37–48

Liu S, Guo Z, Zhang Z, Li Q, Zheng H (2004) Nature of the Precambrian metamorphic blocks in the eastern segment of Central Tianshan: Constraint from geochronology and Nd isotopic geochemistry. Sci China Ser D Earth Sci 47(12):1085–1094

Liu H, Zi J, Cawood PA, Cui X, Zhang L (2020) Reconstructing South China in the Mesoproterozoic and its role in the Nuna and Rodinia supercontinents. Precambr Res 337:105558

Long X, Wilde SA, Yuan C, Hu A, Sun M (2015) Provenance and depositional age of Paleoproterozoic metasedimentary rocks in the Kuluketage Block, northern Tarim Craton: Implications for tectonic setting and crustal growth. Precambr Res 260:76–90

Ma R, Shu L, Sun J (1997) Tectonic evolution and metallogeny of Eastern Tianshan Mountains. Beijing: Geological Publishing House 1:202 **(in Chinese with English abstract)**

Macpherson CG, Dreher ST, Thirlwall MF (2006) Adakites without slab melting: high pressure differentiation of island arc magma, Mindanao, the Philippines. Earth Planet Sci Lett 243(3–4):581–593

Maniar PD, Piccoli PM (1989) Tectonic discrimination of granitoids. Geol Soc Am Bull 101(5):635–643

Mao Q, Xiao W, Fang T, Wang J, Han C, Sun M, Yuan C (2012) Late Ordovician to early Devonian adakites and Nb-enriched basalts in the Liuyuan area, Beishan, NW China: implications for early Paleozoic slab-melting and crustal growth in the southern Altaids. Gondwana Res 22(2):534–553

Mao Q, Yu M, Xiao W, Windley BF, Li Y, Wei X, Zhu J, Lü X (2018) Skarn-mineralized porphyry adakites in the Harlik arc at Kalatage, E. Tianshan (NW China): Slab melting in the Devonian-early Carboniferous in the southern Central Asian Orogenic Belt. J Asian Earth Sci 153:365–378

Mao Q, Wang J, Xiao W, Windley BF, Schulmann K, Yu M, Fang T, Li Y (2019) Mineralization of an intra-oceanic arc in an accretionary orogen: Insights from the Early Silurian Honghai volcanogenic massive sulfide Cu-Zn deposit and associated adakites of the Eastern Tianshan (NW China). Geol Soc Am Bull 131(5–6):803–830

Mao Q, Ao S, Windley BF, Wang J, Li Y, Xiao W (2021a) Middle Triassic lower crust-derived adakitic magmatism: Thickening of the Dananhu intra-oceanic arc and its implications for arc–arc amalgamation in the Eastern Tianshan (NW China). Geol J 56(6):3137–3154

Mao Q, Ao S, Windley BF, Zhang Z, Song D, Je Z, Wan B, Tan W, Han C, Xiao W (2021b) Petrogenesis of Late Carboniferous-Early Permian mafic-ultramafic-felsic complexes in the eastern Central Tianshan, NW China: The result of subduction-related transtension? Gondwana Res 95:72–87

Martin H (1999) Adakitic magmas: modern analogues of Archaean granitoids. Lithos 46(3):411–429

Mossakovskii A, Ruzhentsev S, Samygin S, Kheraskova T (1993) Geotektonika, No. 6. In, vol., p 3

Muhtar M, Wu C, Santosh M, Lei R, Gu L, Wang S, Gan K (2020) Late Paleozoic tectonic transition from subduction to post-collisional extension in Eastern Tianshan, Central Asian Orogenic Belt. Geol Soc Am Bull 132(7–8):1756–1774

Muir R, Weaver S, Bradshaw J, Eby G, Evans J (1995) The Cretaceous Separation Point batholith, New Zealand: granitoid magmas formed by melting of mafic lithosphere. J Geol Soc 152(4):689–701

Nie F (2002) Geological features and origin of the Zhaobishan gold deposit in the Beishan region, northwest China. Chinese J Geol 37:207–218 ((**in Chinese with English abstract**))

Paton C, Hellstrom J, Paul B, Woodhead J, Hergt J (2011) Lolite: Freeware for the visualisation and processing of mass spectrometric data. Journal of Analytical Atomic Spectrometry 26:2508–2518

Peacock SM, Rushmer T, Thompson AB (1994) Partial melting of subducting oceanic crust. Earth Planet Sci Lett 121(1–2):227–244

Peccerillo A, Taylor S (1976) Geochemistry of Eocene calc-alkaline volcanic rocks from the Kastamonu area, northern Turkey. Contrib Mineral Petrol 58(1):63–81

Petford N, Atherton M (1996) Na-rich partial melts from newly underplated basaltic crust: The Cordillera Blanca Batholith. Peru J Petrol 37(6):1491–1521

Reich PB, Wright IJ, Cavender-Bares J, Craine J, Oleksyn J, Westoby M, Walters M (2003) The evolution of plant functional variation: traits, spectra, and strategies. Int J Plant Sci 164(S3):S143–S164

Rogers G, Saunders A, Terrell D, Verma S, Marriner G (1985) Geochemistry of Holocene volcanic rocks associated with ridge subduction in Baja California. Mexico Nat 315(6018):389–392

Rytsk EY, Kovach V, Kovalenko V, Yarmolyuk V (2007) Structure and evolution of the continental crust in the Baikal Fold Region. Geotectonics 41(6):440–464

Sajona FG, Maury RC, Bellon H, Cotten J, Defant MJ, Pubellier M (1993) Initiation of subduction and the generation of slab melts in western and eastern Mindanao, Phillippines. Geology 21(11):1007–1010

Şengör A, Natalin B, Burtman V (1993) Evolution of the Altaid tectonic collage and Palaeozoic crustal growth in Eurasia. Nature 364(6435):299–307

Sengör AC, Natal'In BA (1996) Turkic-type orogeny and its role in the making of the continental crust. Annu Rev Earth Planet Sci 24(1):263–337

Shu L, Yu J, Charvet J, Laurent-Charvet S, Sang H, Zhang R (2004) Geological, geochronological and geochemical features of granulites in the Eastern Tianshan, NW China. J Asian Earth Sci 24(1):25–41

Song S, Xiao W, Windley B F, Collins A S, Chen Y, Zhang J, Schulmann K, Han C, Wan B, Ao S, Zhnag Z, Song D, Li R (2020) Late Paleozoic Chingiz and Saur Arc amalgamation in West Junggar (NW China): Implications for accretionary tectonics in the southern Altaids. Tectonics 39: e2019TC005781.

Spencer C, Roberts N, Santosh M (2017) Growth, destruction, and preservation of Earth's continental crust. Earth Sci Rev 172:87–106

Sun S, McDonough WF (1989) Chemical and isotopic systematics of oceanic basalts: implications for mantle composition and processes. Geol Soc London Spec Public 42(1):313–345

Thorkelson DJ, Breitsprecher K (2005) Partial melting of slab window margins: genesis of adakitic and non-adakitic magmas. Lithos 79(1–2):25–41

Wan B, Li S, Xiao W, Windley BF (2018) Where and when did the Paleo-Asian ocean form? Precambr Res 317:241–252

Wang Q, Xu J, Zhao Z, Bao Z, Xu W, Xiong X (2004) Cretaceous high-potassium intrusive rocks in the Yueshan-Hongzhen area

of east China: Adakites in an extensional tectonic regime within a continent. Geochem J 38(5):417–434
Wang D, Zhang X, Fu H (2006) SHRIMP U-Pb dating of zircons from the north Xiaoyanchi monzodiorite, East Tianshan, Xinjiang. China Geol Bull China 25(8):966–968
Wang Q, Wyman DA, Xu J, Jian P, Zhao Z, Li C, Xu W, Ma J, He B (2007) Early Cretaceous adakitic granites in the Northern Dabie Complex, central China: implications for partial melting and delamination of thickened lower crust. Geochim Cosmochim Acta 71(10):2609–2636
Wang Y, Wang J, Wang L, Long L, Tang P, Liao Z, Zhang H, Shi Y (2012) The Tuerkubantao ophiolite mélange in Xinjiang, NW China: new evidence for the Erqis suture zone. Geosci Front 3(5):587–602
Wang B, Liu H, Shu L, Jahn B-m, Chung S-l, Zhai Y, Liu D (2014a) Early Neoproterozoic crustal evolution in northern Yili Block: insights from migmatite, orthogneiss and leucogranite of the Wenquan metamorphic complex in the NW Chinese Tianshan. Precambr Res 242:58–81
Wang F, Xu W, Gao F, Zhang H, Pei F, Zhao L, Yang Y (2014b) Precambrian terrane within the Songnen-Zhangguangcai Range Massif, NE China: evidence from U-Pb ages of detrital zircons from the Dongfengshan and Tadong groups. Gondwana Res 26(1):402–413
Wang Q, Hao L, Zhang X, Zhou J, Wang J, Li Q, Ma L, Zhang L, Qi Y, Tang G (2020) Adakitic rocks at convergent plate boundaries: Compositions and petrogenesis. Sci China Earth Sci 63(12):1992–2016
Wang P, Zhao G, Cawood PA, Han Y, Yu S, Liu Q, Yao J, Zhang D (2022) South Tarim tied to north India on the periphery of Rodinia and Gondwana and implications for the evolution of two supercontinents. Geology 50(2):131–136
Wen B, Evans DA, Wang C, Li Y, Jing X (2018) A positive test for the Greater Tarim Block at the heart of Rodinia: Mega-dextral suturing of supercontinent assembly. Geology 46(8):687–690
Windley BF, Alexeiev D, Xiao W, Kröner A, Badarch G, (2007) Tectonic models for accretion of the Central Asian Orogenic Belt. J Geol Soc 164(1):31–47
Windley B, Maruyama S, Xiao W (2010) Delamination/thinning of sub-continental lithospheric mantle under Eastern China: The role of water and multiple subduction. Am J Sci 310(10):1250–1293
Wu C, Zhang Z, Zaw K, Della-Pasqua F, Tang J, Zheng Y, Wang C, San J (2006) Geochronology, geochemistry and tectonic significances of the Hongyuntan granitoids in the Qoltag area. Eastern Tianshan Acta Petrologica Sinica 22(5):1121–1134
Xiao WJ, Santosh M (2014) The western Central Asian Orogenic Belt: a window to accretionary orogenesis and continental growth. Gondwana Res 25(4):1429–1444
Xiao S, Bao H, Wang H, Kaufman AJ, Zhou C, Li G, Yuan X, Ling H (2004) The Neoproterozoic Quruqtagh Group in Eastern Chinese Tianshan: evidence for a post-Marinoan glaciation. Precambr Res 130(1–4):1–26
Xiao WJ, Mao QG, Windley BF, Han CM, Qu JF, Zhang J, Ao SJ, Guo QQ, Cleven NR, Lin SF (2010) Paleozoic multiple accretionary and collisional processes of the Beishan orogenic collage. Am J Sci 310(10):1553–1594
Xiao WJ, Sun M, Santosh M (2015a) Continental reconstruction and metallogeny of the Circum-Junggar areas and termination of the southern Central Asian Orogenic Belt. Geosci Front 6(2):137–140
Xiao WJ, Windley BF, Sun S, Li JL, Huang BC, Han CM, Yuan C, Sun M, Chen HL (2015b) A tale of amalgamation of three Permo-Triassic collage systems in Central Asia: Oroclines, sutures, and terminal accretion. Annu Rev Earth Planet Sci 43:477–507
Xiao W, Windley BF, Han C, Liu W, Wan B, Zhang JE, Ao S, ZhangZ SD (2018) Late Paleozoic to early Triassic multiple roll-back and oroclinal bending of the Mongolia collage in Central Asia. Earth Sci Rev 186:94–128
Xiong X, Zhao Z, Bai Z, Mei H, Wang Y, Wang Q, Xu J, Niu H, Bao Z (2001) Adakite-type sodium-rich rocks in Awulale Mountain of west Tianshan: Significance for the vertical growth of continental crust. Chin Sci Bull 46(10):811–817
Xu J, Shinjo R, Defant MJ, Wang Q, Rapp RP (2002) Origin of Mesozoic adakitic intrusive rocks in the Ningzhen area of east China: partial melting of delaminated lower continental crust? Geology 30(12):1111–1114
Xu X, Wang H, Li P, Chen J, Ma Z, Zhu T, Wang N, Dong Y (2013) Geochemistry and geochronology of Paleozoic intrusions in the Nalati (Narati) area in western Tianshan, Xinjiang, China: Implications for Paleozoic tectonic evolution. J Asian Earth Sci 72:33–62
Yan C, Shu L, Faure M, Chen Y, Huang R (2019) Time constraints on the closure of the Paleo-South China Ocean and the Neoproterozoic assembly of the Yangtze and Cathaysia blocks: Insight from new detrital zircon analyses. Gondwana Res 73:175–189
Yang X, Deloule E, Xia Q, Fan Q, Feng M (2008) Water contrast between Precambrian and Phanerozoic continental lower crust in eastern China. J Geophys Res Solid Earth. https://doi.org/10.1029/2007JB005541
Yang G, Li Y, Xiao W, Tong L (2015) OIB-type rocks within West Junggar ophiolitic mélanges: Evidence for the accretion of seamounts. Earth Sci Rev 150:477–496
Yang S, Humayun M, Salters VJ (2020) Elemental constraints on the amount of recycled crust in the generation of mid-oceanic ridge basalts (MORBs). Science Advances 6(26):eaba2923
Yao J, Cawood PA, Shu L, Zhao G (2019) Jiangnan Orogen, South China: A~ 970–820 Ma Rodinia margin accretionary belt. Earth Sci Rev 196:102872
Yao J, Cawood PA, Zhao G, Han Y, Xia X, Liu Q, Wang P (2021) Mariana-type ophiolites constrain the establishment of modern plate tectonic regime during Gondwana assembly. Nat Commun 12(1):1–10
Yogodzinski G, Kay R, Volynets O, Koloskov A, Kay S (1995) Magnesian andesite in the western Aleutian Komandorsky region: implications for slab melting and processes in the mantle wedge. Geol Soc Am Bull 107(5):505–519
Zhang L, Ellis DJ, Jiang W (2002) Ultrahigh-pressure metamorphism in western Tianshan, China: Part I. Evidence from inclusions of coesite pseudomorphs in garnet and from quartz exsolution lamellae in omphacite in eclogites. Am Mineral 87(7):853–860
Zhang Z, Gu L, Wu C, Li W, Xi A, Wang S (2005) Zircon SHRIMP dating for the Weiya pluton, eastern Tianshan: Its geological implications. Acta Geologica Sinica (English Edition) 79(4):481–490
Zhang C, Li X, Li Z, Lu S, Ye H, Li H (2007a) Neoproterozoic ultramafic-mafic-carbonatite complex and granitoids in Quruqtagh of northeastern Tarim Block, western China: Geochronology, geochemistry and tectonic implications. Precambr Res 152(3–4):149–169
Zhang Z, Gu L, Wu C, Zhai J, Li W, Tang J (2007b) Early Indosinian Weiya gabbro in Eastern Tianshan, China: Elemental and Sr-Nd-O isotopic geochemistry, and its tectonic implications. Acta Geologica Sinica (english Edition) 81(3):424–432
Zhao G (2015) Jiangnan Orogen in South China: Developing from divergent double subduction. Gondwana Res 27(3):1173–1180
Zhao J, Mooney WD, Zhang X, Li Z, Jin Z, Okaya N (2006) Crustal structure across the Altyn Tagh Range at the northern margin of the Tibetan Plateau and tectonic implications. Earth Planet Sci Lett 241(3–4):804–814

Zhao G, Li S, Sun M, Wilde SA (2011) Assembly, accretion, and break-up of the Palaeo-Mesoproterozoic Columbia supercontinent: Record in the North China Craton revisited. Int Geol Rev 53(11–12):1331–1356

Zhao P, He J, Deng C, Chen Y, Mitchell RN (2021) Early Neoproterozoic (870–820 Ma) amalgamation of the Tarim craton (northwestern China) and the final assembly of Rodinia. Geology 49(11):1277–1282

Zuo G, Zhang S, He G, Zhang Y (1991) Plate tectonic characteristics during the early Paleozoic in Beishan near the Sino-Mongolian border region. China Tectonophys 188(3–4):385–392

Zuo G (1990) Plate tectonics and metallogenic regularities in Beishan region. Beijing Univ Pub House: 1–210 **(in Chinese with English abstract)**